The structure of molten CuCl, CuI and their mixtures as investigated by using neutron diffraction

2009 J. Phys.: Condens. Matter 21 075104

(http://iopscience.iop.org/0953-8984/21/7/075104)

J. Phys.: Condens. Matter **21** (2009) 075104 (9pp) doi:10.1088/0953-8984/21/7/075104

The structure of molten CuCl, CuI and their mixtures as investigated by using neutron diffraction

James W E Drewitt[1], Philip S Salmon[1], Shin'ichi Takeda[2] and Yukinobu Kawakita[2]

[1] Department of Physics, University of Bath, Bath BA2 7AY, UK
[2] Department of Physics, Faculty of Science, Kyushu University, Ropponmatsu, Fukuoka 810-8560, Japan

Received 4 November 2008, in final form 12 December 2008
Published 13 January 2009
Online at stacks.iop.org/JPhysCM/21/075104

Abstract
The structure of molten CuCl, CuI and their mixtures $(CuCl)_x(CuI)_{1-x}$ with $x = 0.294$, 0.576, 0.801 was studied by using neutron diffraction. The results are discussed by reference to the information that is available on the structure of CuCl and CuI from experiment, theory and computer simulation. The comparison points to a need for more realistic models for the CuCl–CuI system which should take into account the presence of chemical bonds that have been found in CuI by the application of *ab initio* molecular dynamics methods.

(Some figures in this article are in colour only in the electronic version)

1. Introduction

The copper halides CuX (X = Cl, Br, I) belong to an important class of systems that exhibit fast-ion (or superionic) conductivity with Cu^+ ions as the mobile species [1–5]. For example, at ambient temperature and pressure CuI forms the γ-phase which has a zinc-blende structure in which the anions form a face centred cubic (fcc) sublattice. When the temperature is increased to 643 K, a transformation occurs into the β-phase where the anions form a slightly distorted hexagonal close packed (hcp) sublattice. A further transition into the superionic α-phase occurs at 673 K, where the anions again form an fcc sublattice, and the system melts from this phase at 878 K [6]. Tracer diffusion measurements show an increase in the self-diffusion coefficient of Cu^+ from the order of 10^{-7} cm^2 s^{-1} for the γ-phase, to the order of 10^{-6} cm^2 s^{-1} for the β-phase and to a liquid-like value of 3.5×10^{-5} cm^2 s^{-1} for the α-phase at 834 K [7, 8]. The ionic conductivity of the superionic and molten phases is comparable at $\approx$1 Ω^{-1} cm^{-1} [3, 9]. By comparison, the ambient γ-phase of CuCl also has a zinc-blende structure and this transforms at 681 K to the β-phase, which has a wurtzite structure where the anions form an hcp sublattice, from which the system melts at 703 K. Although the ionic conductivity of β-CuCl is relatively high at $\approx$0.1 Ω^{-1} cm^{-1} [9] and the Cu^+ self-diffusion coefficient assumes liquid-like values [10], it is often not regarded as a true superionic phase since the cations are reported to have only a limited occupation of the interstitial sites [5, 11]. The application of a pressure $\gtrsim$2 kbar at a temperature $\gtrsim$700 K does, however, lead to such a phase in which the anions form a body centred cubic (bcc) sublattice as adopted by the ambient pressure superionic phases of α-AgI and α-CuBr [11]. In addition, copper halides can be used to modify network glasses to make materials such as CuI–$CuPO_3$ and CuI–PbI_2–As_2Se_3 that have a high ionic conductivity, giving them application as solid state electrochemical devices [12–17]. It is therefore important to understand the structure of copper halides in order to give insight into their basic physico-chemical properties and to have a guide in making realistic models for these and other related materials.

The object of the present paper is to make a systematic study of the structure of molten $(CuCl)_x(CuI)_{1-x}$ ($0 \leqslant x \leqslant 1$) mixtures by using neutron diffraction. The phase diagram of this system is given in [18] and shows a minimum in the liquidus curve at the composition $x = 0.58$ where melting takes place at a temperature of 557 K. The CuX compounds are intermediate between ionic and covalent materials and the ionicity of the bonding is anticipated to decrease with increasing anion radius [19]. Part of the motivation for the present study is therefore provided by a desire to understand the effect on the system properties of the competition provided

by mixing anions that have the same charge but unequal size. It is also interesting to see if interatomic potentials can be developed that are transferrable [20] and can therefore account for the basic structural and dynamical properties of the mixtures without the need to make an ad hoc parametrization of the potential parameters [21, 22].

The structure and other properties of molten CuCl [23–44] and CuI [31–33, 35–52] have been extensively studied by experiment, theory and computer simulation, thus providing a benchmark for work on their mixtures. In particular, the full set of partial structure factors for molten CuCl was measured by Page and Mika [23] in an early use of the method of isotopic substitution in neutron diffraction and the results were subsequently improved upon by Eisenberg *et al* [28]. There have also been several attempts to measure the full set of partial structure factors for molten CuI by using either anomalous x-ray scattering [46] or neutron and x-ray diffraction [50, 51] in combination with the reverse Monte Carlo (RMC) method [53]. For molten CuCl–CuBr mixtures, the structure has been investigated by using neutron diffraction [54] and the magnetic susceptibility, ultrasonic velocity, sound attenuation and density have also been measured [37, 55]. The results show deviations from the behaviour expected for an ideal mixture. The magnetic susceptibility for molten CuCl–CuI mixtures has also been measured and shows a linear dependence on the composition [37].

2. Theory

In a neutron diffraction experiment on liquid $(CuCl)_x(CuI)_{1-x}$ the coherent scattered intensity can be represented by the total structure factor [56]

$$F(k) = \sum_{\alpha=1}^{n}\sum_{\beta=1}^{n} c_\alpha c_\beta b_\alpha b_\beta \left[S_{\alpha\beta}(k) - 1\right] \tag{1}$$

where α and β denote the chemical species, $n = 3$ is the number of different chemical species, c_α and b_α represent the atomic fraction and coherent neutron scattering length of chemical species α, respectively, $S_{\alpha\beta}(k)$ is a partial structure factor and k is the scattering vector. The corresponding real-space information is provided by the total pair distribution function which is obtained from the Fourier transform relation

$$G(r) = \frac{1}{2\pi^2 r n_0}\int_0^\infty \mathrm{d}k\, kF(k)\sin(kr) \tag{2}$$

$$= \sum_{\alpha=1}^{n}\sum_{\beta=1}^{n} c_\alpha c_\beta b_\alpha b_\beta \left[g_{\alpha\beta}(r) - 1\right] \tag{3}$$

where n_0 is the atomic number density, $g_{\alpha\beta}(r)$ is a partial pair distribution function, and r is a distance in real space. The low r limiting value of this function is given by $G(r = 0) = -\sum_\alpha \sum_\beta c_\alpha c_\beta b_\alpha b_\beta$. The mean coordination number of atoms of type β, contained in a volume defined by two concentric spheres of radii r_i and r_j centred on an atom of type α, is given by

$$\bar{n}_\alpha^\beta = 4\pi n_0 c_\beta \int_{r_i}^{r_j} \mathrm{d}r\, g_{\alpha\beta}(r) r^2. \tag{4}$$

In practice, the measured reciprocal space data sets will be truncated at some finite maximum value $k_{\max}$ owing to the limited measurement window function $M(k)$ of the diffractometer. In consequence, equation (2) needs to be modified and it is convenient to re-write it as

$$rG'(r) = \frac{1}{2\pi^2 n_0}\int_0^\infty \mathrm{d}k\, kF(k)M(k)\sin(kr) = rG(r)\otimes M(r) \tag{5}$$

where $\otimes$ denotes the one-dimensional convolution operator. In this expression the function $rG(r)$ is convoluted with a symmetrical $M(r)$ function. For example, the measurement window is usually represented by the step function $M(k) = 1$ for $|k| \leqslant k_{\max}$, $M(k) = 0$ for $|k| > k_{\max}$ whence $M(r) = \sin(k_{\max}r)/\pi r$. Alternatively, the adoption of a Lorch [57] modification function $M(k) = \sin(ak)/(ak)$ for $|k| \leqslant k_{\max}$, $M(k) = 0$ for $|k| > k_{\max}$ gives $M(r) = [\mathrm{Si}(\pi(r + a)/a) - \mathrm{Si}(\pi(r - a)/a)]/2\pi a$ where $a = \pi/k_{\max}$ and the sine integral $\mathrm{Si}(x) \equiv \int_0^x \sin(t)/t\,\mathrm{d}t$ [58]. If the oscillations in the structure factor have not ceased before $k_{\max}$ then an application of the Lorch or related modification function will give a smoother pair correlation function at all r values by comparison with the use of a step modification function but at the expense of a loss in resolution of the first peaks in r space.

We note that the finite k space resolution function of the diffractometer will also have an effect on the shape of the measured total pair distribution function [58]. In the following this effect will not be taken into account, owing to the difficulty in making a reliable correction [59], but it is not anticipated to be particularly large for the liquids under investigation.

3. Experimental details

The $(CuCl)_x(CuI)_{1-x}$ samples were prepared by weighing CuCl (Aldrich 99.995+%) and CuI (Aldrich 99.999%) in the correct proportions in a dry nitrogen filled glove box. They were then sealed under vacuum in silica ampoules (7 mm inner diameter and 1 mm wall thickness) that had been cleaned (by using chromic acid and distilled water) and thoroughly dried. The neutron diffraction experiment was made using the SANDALS instrument at the ISIS pulsed neutron source [60] and diffraction patterns were taken for each sample in its container in the furnace, an empty container in the furnace at several high temperatures, the empty furnace, the empty instrument, and a vanadium rod of diameter 8.35 mm in the furnace for normalization purposes. The data analysis was made using the program GUDRUN [61] which makes the necessary corrections detector by detector before merging the results to give a total structure factor $F(k)$. The maximum neutron energy used in the data analysis was chosen to avoid the visible neutron resonances of iodine [62]. It was checked that each $F(k)$ obeys the sum-rule relation $\int_0^\infty F(k)k^2\,\mathrm{d}k = 2\pi^2 n_0 G(0)$ and gives rise to a well-behaved real-space function $G'(r)$ [56, 63]. This should oscillate about the calculated value for $G(0)$ at small r values and, when the oscillations are set to this limiting value, the Fourier back transform of $G'(r)$ should be in good overall agreement with the original reciprocal space data set. The coherent neutron

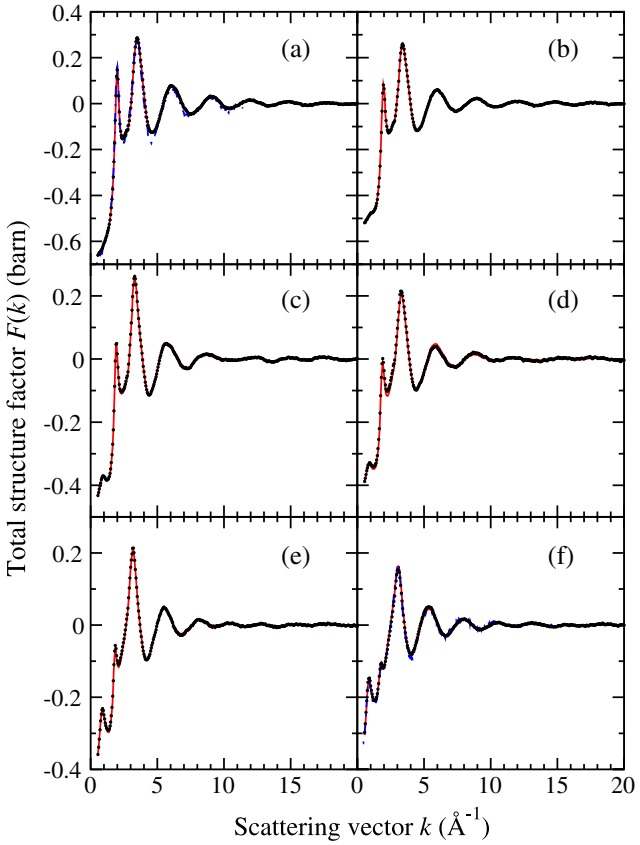

Figure 1. The measured total structure factors $F(k)$ for (a) CuCl at 733 K, (b) $(CuCl)_{0.801}(CuI)_{0.199}$ at 693 K, (c) $(CuCl)_{0.576}(CuI)_{0.424}$ at 613 K, (d) $(CuCl)_{0.576}(CuI)_{0.424}$ at 873 K, (e) $(CuCl)_{0.294}(CuI)_{0.706}$ at 773 K and (f) CuI at 933 K. The solid circles represent the measured data points and the symbol size is larger than the statistical error. The solid (red) curves are the Fourier back-transforms of the corresponding total pair distribution functions $G'(r)$ given in figure 2 after the unphysical oscillations at r values smaller than the distance of closest approach between the centres of two atoms are set to the calculated $G(r = 0)$ limit. The broken (blue) curve gives the $F(k)$ function measured for (a) CuCl at 773 K by Eisenberg *et al* [28] or (f) CuI at 923 K by Takeda *et al* [50].

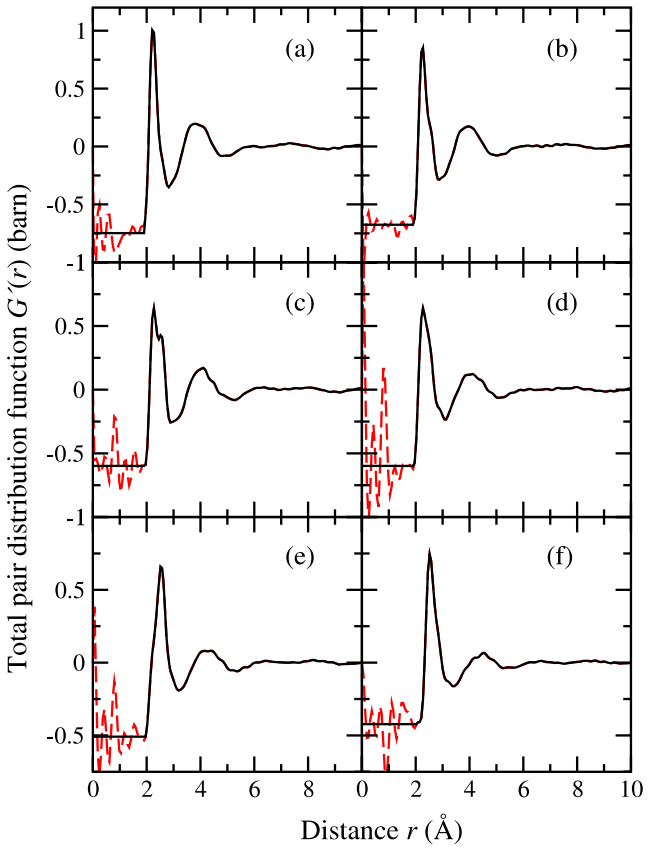

Figure 2. The total pair distribution functions $G'(r)$ for (a) CuCl at 733 K, (b) $(CuCl)_{0.801}(CuI)_{0.199}$ at 693 K, (c) $(CuCl)_{0.576}(CuI)_{0.424}$ at 613 K, (d) $(CuCl)_{0.576}(CuI)_{0.424}$ at 873 K, (e) $(CuCl)_{0.294}(CuI)_{0.706}$ at 773 K and (f) CuI at 933 K as obtained by Fourier transforming the $F(k)$ shown in figure 1 with $k_{max} = 20$ Å^{-1}. The broken (red) curves show the extent of the unphysical oscillations at r values smaller than the distance of closest approach between the centres of two atoms.

scattering lengths are $b_{Cu} = 7.718(4)$, $b_{Cl} = 9.5770(8)$ and $b_I = 5.28(2)$ fm [64].

The temperatures of the molten materials and the corresponding number densities are summarized in table 1. For the CuCl–CuI mixtures, the number density at temperature T (in °C) was deduced from the measured molar volumes V_M of CuCl and CuI [65]

$$V_M(\text{CuCl})\ (\text{cm}^3\ \text{mol}^{-1}) = 24.34(1 + 2.10 \times 10^{-4}T + 3.24 \times 10^{-8}T^2), \quad (6)$$

$$V_M(\text{CuI})\ (\text{cm}^3\ \text{mol}^{-1}) = 34.71(1 + 3.83 \times 10^{-4}T - 5.12 \times 10^{-8}T^2) \quad (7)$$

by the application of Vegard's law where

$$V_M((\text{CuCl})_x(\text{CuI})_{1-x}) = xV_M(\text{CuCl}) + (1-x)V_M(\text{CuI}). \quad (8)$$

For molten CuCl–CuBr mixtures, the measured molar volume of the mixture is larger than the value calculated by using Vegard's law with a maximum deviation of ≃3% [55].

4. Results

The measured total structure factors, $F(k)$, for the $(CuCl)_x(CuI)_{1-x}$ melts are shown in figure 1 and the corresponding total pair distribution functions, $G'(r)$, are shown in figure 2. The latter were obtained by using equation (5) after $F(k)$ was spline fitted and truncated either by using a step modification function $M(k)$ with $k_{max} = 20$ Å^{-1} ($x = 1$, 0.801, 0.576 at 613 K) or more smoothly by applying a cosine window function to the region between ≈18 and 20 Å^{-1} ($x = 0$, 0.294, 0.576 at 873 K). Use of this large k_{max} value means that $G'(r) \simeq G(r)$ at all r values. The first few peak and/or shoulder positions in the $F(k)$ and $G'(r)$ functions are summarized in table 1. The measured $F(k)$ functions for liquid CuCl and CuI are in good overall agreement with previous neutron diffraction results (see figures 1(a) and (f)) [28, 50].

The measured $F(k)$ for molten CuCl features a sharp principal peak at 2.00(2) Å^{-1}. By comparison, the $F(k)$ for molten CuI shows a small principal peak at 1.79(2) Å^{-1} but features a so-called first sharp diffraction peak (FSDP) at 0.88(2) Å^{-1} which is a signature of ordering on an intermediate length scale [66]. As shown by the comparison

Table 1. Details of the various $(CuCl)_x(CuI)_{1-x}$ liquids investigated by neutron diffraction. The temperature T and corresponding number density n_0 are given together with the positions k_1, k_2 and k_3 of the first three peaks in the measured $F(k)$ functions for the range $0 \leqslant k$ (Å^{-1}) $\leqslant 3.5$ (see figure 1) and the positions r_1, r_2 and r_3 of the first three peaks or shoulders in the measured $G'(r)$ functions for the range $0 \leqslant r$ (Å) $\lesssim 4.5$ (see figure 2). For CuCl ($x = 1$) there is no FSDP in $F(k)$ at $\simeq 1$ Å^{-1} and for CuI ($x = 0$) the first main peak in $G'(r)$ occurs at 2.53(2) Å and is asymmetric but the shoulder at 2.84(2) Å is not listed.

			$F(k)$			$G'(r)$		
x	T (K)	n_0 (Å^{-3})	k_1 (Å^{-1})	k_2 (Å^{-1})	k_3 (Å^{-1})	r_1 (Å)	r_2 (Å)	r_3 (Å)
1	733(3)	0.0448(5)	—	2.00(2)	3.49(2)	2.23(2)	2.57(2)	3.80(3)
0.801	693(3)	0.0411(3)	1.07(2)	1.96(2)	3.39(2)	2.25(2)	2.57(2)	3.95(3)
0.576	613(3)	0.0381(3)	0.94(2)	1.93(2)	3.30(2)	2.27(2)	2.57(2)	4.09(3)
0.576	873(3)	0.0357(3)	0.92(2)	1.90(2)	3.27(2)	2.28(2)	2.58(2)	4.10(3)
0.294	773(3)	0.0342(3)	0.90(2)	1.86(2)	3.18(2)	2.25(2)	2.54(2)	4.14(3)
0	933(3)	0.0282(3)	0.88(2)	1.79(2)	3.04(2)	—	2.53(2)	4.52(3)

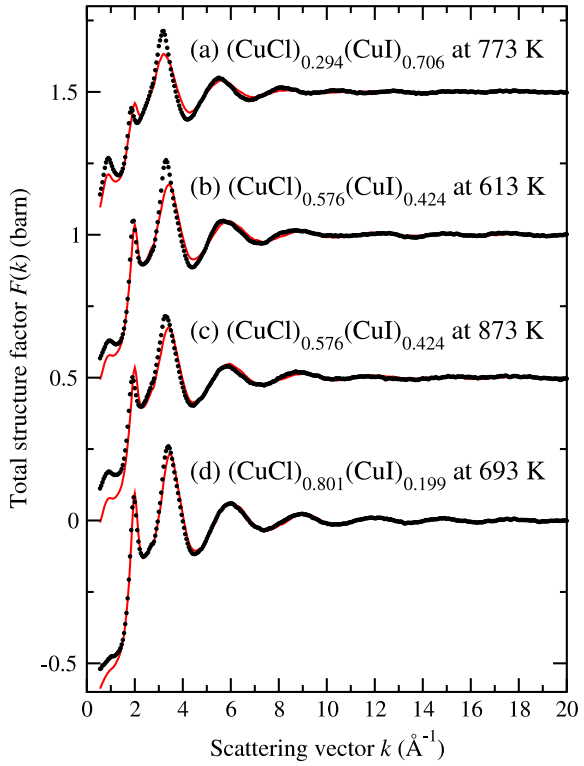

Figure 3. The total structure factors $F(k)$ for the $(CuCl)_x(CuI)_{1-x}$ mixtures given in figure 1 (solid circles) as compared to their reconstruction $^{rec}F(k)$ (solid (red) curves) from the measured total structure factors for CuCl at 733 K, $^{CuCl}F(k)$, and CuI at 933 K, $^{CuI}F(k)$, where $^{rec}F(k) = x^{CuCl}F(k) + (1-x)^{CuI}F(k)$. The data for (a) $(CuCl)_{0.294}(CuI)_{0.706}$ at 773 K, (b) $(CuCl)_{0.576}(CuI)_{0.424}$ at 613 K and (c) $(CuCl)_{0.576}(CuI)_{0.424}$ at 873 K have been shifted vertically by 1.5, 1.0 and 0.5 barn, respectively.

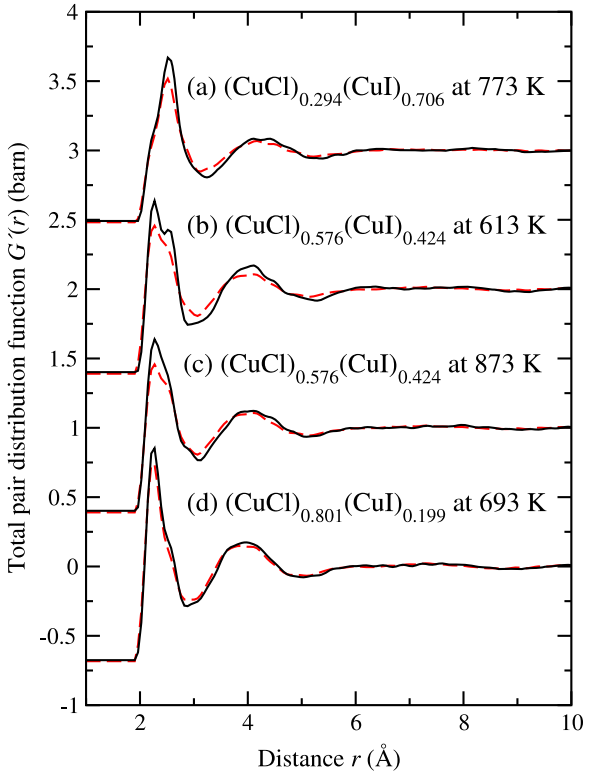

Figure 4. The total pair distribution functions $G'(r)$ for the $(CuCl)_x(CuI)_{1-x}$ mixtures given in figure 2 (solid curves) as compared to their reconstruction $^{rec}G'(r)$ (broken curves) from the measured total pair distribution functions for CuCl at 733 K, $^{CuCl}G'(r)$, and CuI at 933 K, $^{CuI}G'(r)$, where $^{rec}G'(r) = x^{CuCl}G'(r) + (1-x)^{CuI}G'(r)$. The data for (a) $(CuCl)_{0.294}(CuI)_{0.706}$ at 773 K, (b) $(CuCl)_{0.576}(CuI)_{0.424}$ at 613 K and (c) $(CuCl)_{0.576}(CuI)_{0.424}$ at 873 K have been shifted vertically by 3, 2 and 1 barn, respectively.

made in figure 3, the behaviour of the main features in $F(k)$ for the mixtures can be understood by superposing the $F(k)$ functions for the pure CuCl and CuI components. For example, as CuI is added to CuCl an FSDP appears at ≈ 1 Å^{-1} and grows in intensity while shifting to a smaller k value whereas the intensity of the principal peak decreases. It should be noted, however, that although the $F(k)$ functions thus constructed have Cu–X partial structure factors with the correct weighting factors (see equation (1)), they are rough approximations since they do not account for the effects of mixing on the liquid structure and the X–X correlations are given an incorrect weighting.

The first peak in $G'(r)$ at 2.23(2) Å for molten CuCl arises from nearest-neighbour Cu–Cl correlations as shown by the partial pair distribution functions $g_{\alpha\beta}(r)$ that are illustrated in figure 5. Similarly, the first peak in $G'(r)$ at 2.53(2) Å for molten CuI arises from nearest-neighbour Cu–I correlations

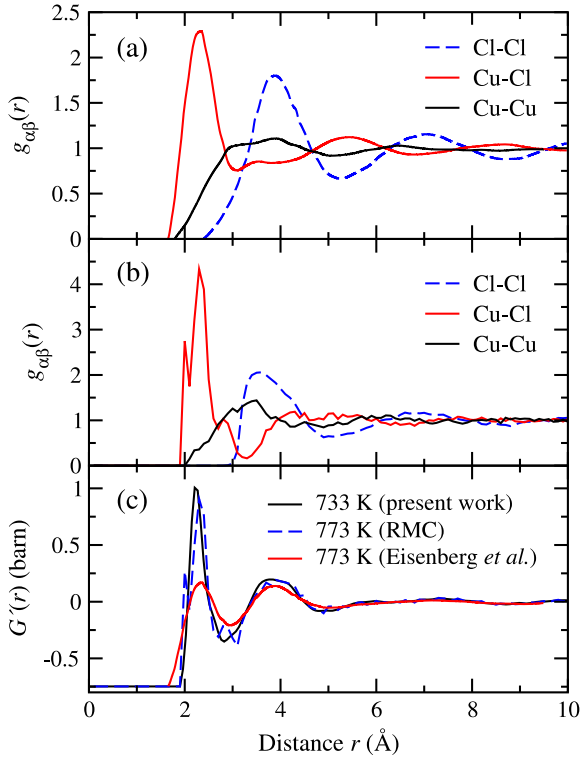

Figure 5. (a) The partial pair distribution functions, $g_{\alpha\beta}(r)$, for molten CuCl at 773 K as obtained by Eisenberg *et al* [28] from the measured $S_{\alpha\beta}(k)$ after the application of a Bartlett modification function (see the text). (b) The $g_{\alpha\beta}(r)$ for molten CuCl at 773 K as obtained by McGreevy and Pusztai [67] from the measured $S_{\alpha\beta}(k)$ of Eisenberg *et al* [28] by using the RMC method. The spike at small r in $g_{\mathrm{CuCl}}(r)$ is an artefact of the RMC analysis procedure. (c) The measured total pair distribution function $G'(r)$ of figure 2 for molten CuCl at 733 K (solid dark (black) curve) as compared with the $G'(r)$ function reconstructed from the $g_{\alpha\beta}(r)$ given in (a) (solid light (red) curve) or (b) (broken (blue) curve) by using equation (3).

(see figure 7). The main features in the $G'(r)$ for the mixtures can be understood by superposing the $G'(r)$ functions for the pure components (see figure 4) e.g. the first peak shifts to a larger r value and decreases in intensity as Cl^- is replaced by I^-, in keeping with an increase in the mean anion radius and a reduction in the mean anion coherent neutron scattering length. For molten $(CuCl)_{0.576}(CuI)_{0.424}$, the ability to resolve the nearest-neighbour Cu–Cl and Cu–I correlations decreases with increasing temperature.

5. Discussion

5.1. Structure of molten CuCl

Two sets of partial pair distribution functions $g_{\alpha\beta}(r)$ for molten CuCl at 773 K are shown in figure 5. Both sets were obtained from the measured partial structure factors $S_{\alpha\beta}(k)$ of Eisenberg *et al* [28], the first by Fourier transforming the $S_{\alpha\beta}(k)$ functions after they had been multiplied by a Bartlett modification function $M(k) = 1 - (|k|/k_{\max})$ for $|k| \leqslant k_{\max}$, $M(k) = 0$ for $|k| > k_{\max}$ with a short $k_{\max}$ value of 9.73 $\mathrm{Å}^{-1}$ chosen to coincide with a node of the $S_{\alpha\beta}(k)$ oscillations [28], and the second by means of the RMC method [67]. The results show that, although there are discrepancies between the two sets of $g_{\alpha\beta}(r)$, molten CuCl is characterized by a relatively featureless $g_{\mathrm{CuCu}}(r)$ function that penetrates deeply into the first peak of $g_{\mathrm{CuCl}}(r)$. In the β-phase from which CuCl melts at ambient pressure, the Cu^+ ions occupy tetrahedral holes in an hcp sublattice of chloride ions [11]. In the liquid, the Cu–Cl coordination number $\bar{n}^{\mathrm{Cl}}_{\mathrm{Cu}} = 3.0(7)$–3.4 [28, 29] which is reported to increase with pressure to ≈3.7 at 1.2 GPa and to ≈5.6 at 18.5 GPa [43]. A comparison is also made in figure 5 between the $G'(r)$ functions derived from both sets of $g_{\alpha\beta}(r)$ and the function measured in the present work for the liquid at a lower temperature of 733 K. The results show that application of the Bartlett modification function leads to a relative broadening of $G'(r)$. The shift observed in the nearest-neighbour peak position between the present work and the RMC results is consistent with the different liquid temperatures.

As pointed out by Page and Mika [23], the structure of liquid CuCl is not typical of a molten salt such as NaCl for which the anion–anion and cation–cation partial structure factors are similar [68]. We note, however, that the structure does resemble molten LiCl [67, 69] in which the Li^+ radius of 0.59 Å is comparable to the Cu^+ radius of 0.60 Å [70]. To try and explain the structure of molten CuCl, Powles [24] proposed a molecular model in which the liquid comprises covalently bonded CuCl diatomic units (also see [26] for a model based on a ternary mixture of atoms and chemical complexes). His approach did not, however, consider the effect of orientational correlations on the partial structure factors [25]. Moreover, the model is inconsistent with the Cu–Cl coordination number of 3.0(7) subsequently measured by Eisenberg *et al* [28], with the high ionic conductivity of the liquid (≈1 Ω^{-1} cm^{-1}), and with the relatively long (≈1 ms) nuclear magnetic resonance relaxation times that have been measured [27, 29]. Nevertheless, there are several properties of the system that point to a partial ionic character for the interactions [28], including its electronegativity [19]. Indeed, it is often argued that the potential barrier to ionic motion between sites is lowered in the case of Ag^+ and Cu^+ owing to their ability to form bonds with substantial mixed (ionic–covalent) character at each intermediate position in their diffusion pathway [1, 2, 5].

More recent models for CuCl and other CuX systems take into account the structure of the solid prior to melting [30]. Many of these models make use of Rahman–Vashishta–Parrinello (RVP) effective interatomic pair potentials [71, 72] in molecular dynamics simulations and in different theoretical approaches where non-integer ionic charges are used to help mimic the effect of 'covalent' interactions [32–34, 36, 38, 39, 41, 44, 73]. The measured $F(k)$ and $G'(r)$ functions for molten CuCl are compared to the molecular dynamics results of [44] in figure 6. In the latter, the RVP potentials were used in a simulation of 1000 ions and the results are very similar to those previously obtained by Stafford *et al* [32]. The comparison of figure 6 shows that the RVP potentials capture the main features in both of the measured functions.

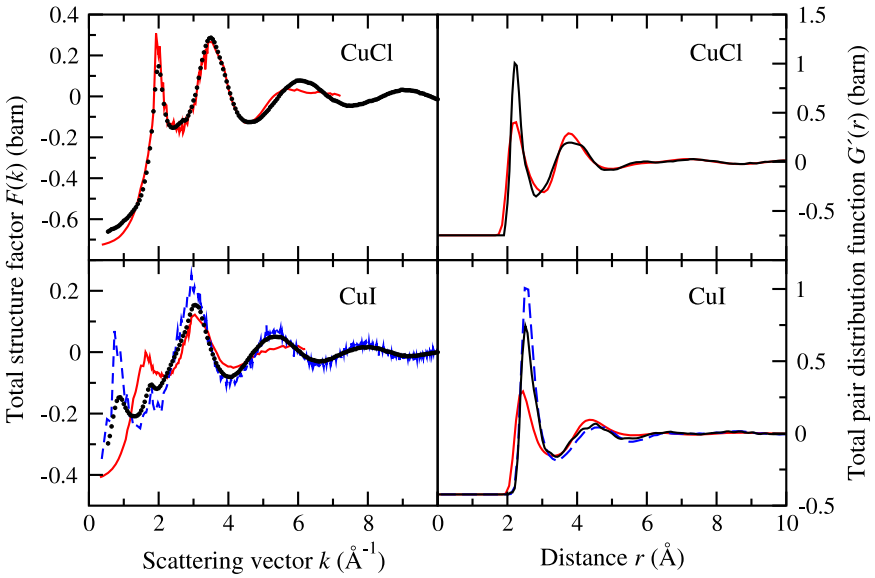

Figure 6. A comparison between the measured $F(k)$ functions (solid circles in the left-hand column) and $G'(r)$ functions (solid dark (black) curves in the right-hand column) for CuCl at 733 K and CuI at 933 K (present work) and the functions obtained from (i) molecular dynamics simulations of CuCl at 773 K and CuI at 938 K using Rahman–Vashishta–Parrinello (RVP) effective interatomic pair potentials (light solid (red) curves) [44] and (ii) *ab initio* molecular dynamics simulations of CuI at 900 K (broken (blue) curves) [48].

5.2. Structure of molten CuI

The partial structure factors for molten CuI have been deduced by applying the RMC method to the diffraction patterns measured by using either anomalous x-ray scattering [46] or a combination of neutron and x-ray diffraction [50, 51]. The short ranged part of $g_{\mathrm{CuI}}(r)$ and $g_{\mathrm{CuCu}}(r)$ has also been measured by using x-ray absorption spectroscopy [47]. The corresponding $g_{\alpha\beta}(r)$ and $S_{\alpha\beta}(k)$ functions are illustrated in figures 7 and 8, respectively. The results show several of the structural characteristics found for molten CuCl (see figure 5) and CuBr [46, 74–76], namely a relatively featureless $g_{\mathrm{CuCu}}(r)$ function that penetrates deeply into the first peak of the Cu–X partial pair distribution function. In the α-phase from which CuI melts at ambient pressure there is a statistical distribution of Cu^+ ions over the tetrahedral interstices of an fcc iodide sublattice [6]. In the liquid, the Cu–I nearest-neighbour distance is 2.53(2) Å and the coordination number $\bar{n}^{\mathrm{I}}_{\mathrm{Cu}} \simeq 2.7$ [51]. The ionic radii of Cu^+, Cl^- and I^- are 0.60, 1.81 and 2.20 Å [70], respectively, while the nearest-neighbour Cu–Cl distance is 2.23(2) Å in liquid CuCl. The discrepancy between the nearest-neighbour Cu–X distance and the sum of the ionic radii is therefore larger for CuI compared with CuCl, in keeping with the smaller ionicity f_i of CuI (0.692 cf 0.746 on the Phillips scale [19]). There is some indication, from the total pair distribution function measured by x-ray diffraction, that the Cu–I coordination number for the liquid gradually increases to a value ≈6 when the pressure is increased beyond 6 GPa [43].

In figure 9 a comparison is made between the measured $g_{\alpha\beta}(r)$ for the superionic α-phase and liquid phase of CuI. The $G'(r)$ functions for the liquid phase at 933 K, the zinc-blende phase at 298 K, and the superionic α-phase at 713 K [77] are also presented. The results show similarities between the local structure of the liquid and the superionic phase, in keeping with the premise made by Ginoza *et al* [30] and the observations made for other systems that melt from a superionic phase like CuBr [76], Ag_2Se [78] and Ag_2Te [79].

As for CuCl, the RVP effective pair potentials with non-integer ionic charges have been used extensively to model the solid and liquid phases of CuI via molecular dynamics and other methods [32, 33, 36, 39, 41, 44, 73, 80–85]. The properties of the superionic and liquid phases have also been investigated by using *ab initio* molecular dynamics simulations [48, 52, 88]. For the liquid, a comparison between the measured $F(k)$ and $G'(r)$ functions and the results obtained from molecular dynamics simulations is given in figure 6 and a comparison between several of the measured and calculated $g_{\alpha\beta}(r)$ and $S_{\alpha\beta}(k)$ functions is given in figures 7 and 8. In these figures the molecular dynamics results of [44], made for a system of 1000 ions using the RVP potentials, are very similar to those previously obtained by Stafford *et al* [32] (in [32] the curves should be interchanged between figures 2 and 3 in order to match the figure captions). The structural and dynamical properties evaluated by using the RVP potentials prove sensitive to the precise values chosen for potential parameters such as the fractional ionic charge [45, 81, 84, 85]. Moreover, the RVP potentials do not reproduce the measured structure of the liquid (see figures 6–8) or the solid α-phase [47, 77, 81] e.g. they do not produce an FSDP in the liquid state $F(k)$ or $S_{\mathrm{CuCu}}(k)$ functions. In comparison, the *ab initio* calculations do lead to an FSDP in these functions, although the associated Cu–Cu pair distribution function is too structured. Empirical three-body potentials have also been used to investigate CuI [49, 86] (and CuCl [87]) but the partial pair distribution functions have not been reported for comparison with experiment.

One problem associated with an effective pair potential approach is the nature of the bonding in CuI. For example,

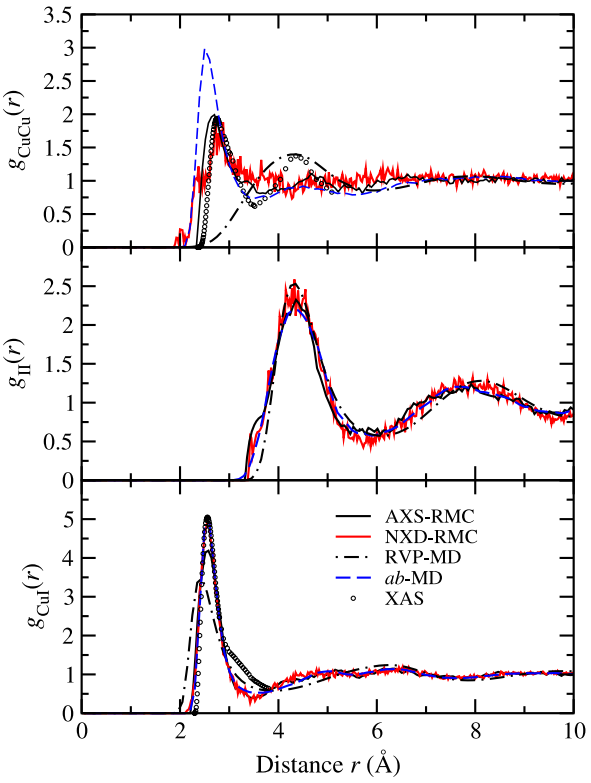

Figure 7. The partial pair distribution functions $g_{\alpha\beta}(r)$ for liquid CuI as obtained by different experimental and molecular dynamics methods. (i) Solid dark (black) curve: CuI at 940 K from anomalous x-ray scattering with RMC (AXS-RMC) [46]. (ii) Solid light (red) curve: CuI at 923 K from neutron and x-ray diffraction with RMC (NXD-RMC) [50]. (iii) Chained (black) curve: CuI at 938 K from molecular dynamics using Rahman–Vashishta–Parrinello effective pair potentials (RVP-MD) [44]. (iv) Broken (blue) curve: CuI at 900 K from *ab initio* molecular dynamics (*ab*-MD) [48]. (v) Open circles: CuI at 903 K from x-ray absorption spectroscopy (XAS) [47].

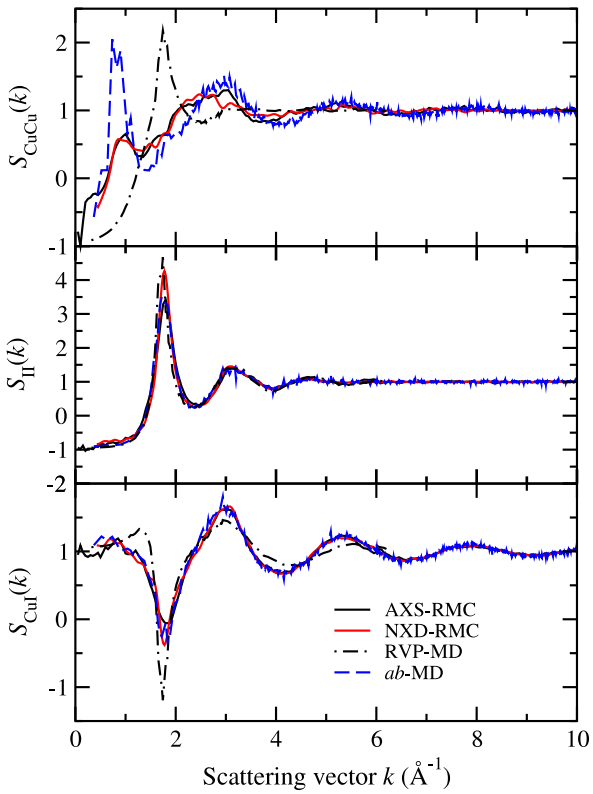

Figure 8. The partial structure factors $S_{\alpha\beta}(k)$ for liquid CuI as obtained by different experimental and molecular dynamics methods. (i) Solid dark (black) curve: CuI at 940 K from anomalous x-ray scattering with RMC (AXS-RMC) [46]. (ii) Solid light (red) curve: CuI at 923 K from neutron and x-ray diffraction with RMC (NXD-RMC) [50]. (iii) Chained (black) curve: CuI at 938 K from molecular dynamics using Rahman–Vashishta–Parrinello effective pair potentials (RVP-MD) [44]. (iv) Broken (blue) curve: CuI at 900 K from *ab initio* molecular dynamics (*ab*-MD) [48].

the *ab initio* molecular dynamics simulations show a change with time in the character of the Cu–I interactions from ionic to covalent as the Cu^+ ions move through the I^- sublattice of the α-phase [88]. For the liquid, the *ab initio* simulations show almost no covalent character for the I–I interactions but a partial covalent character for both the Cu–Cu and Cu–I interactions [48, 52].

5.3. Structure of molten CuCl–CuI mixtures

As a starting point for modelling the structure of the CuCl–CuI mixtures it is necessary to improve existing models for the pure components. One approach would be to add induced dipole polarization effects to the rigid-ion RVP pair potentials, as adopted by Bitrián *et al* for molten AgBr and AgI where non-integer ionic charges were employed [89, 90]. Alternatively, it may be possible to understand the basic properties of CuCl and CuI within the framework of a fully ionic picture for the interatomic interactions based on discrete closed-shell ions with integer charges, where 'covalent' effects may be explained in terms of the ion polarization, compression and deformation [20, 91]. However, the ionicity of the bonding decreases with increasing anion radius [19] and the *ab initio* molecular dynamics models of Shimojo and co-workers for CuI point to the formation of chemical bonds that involve the sharing of electrons between atoms [48, 52, 88]. It may therefore prove necessary to employ *ab initio* methods in order to fully understand the properties of CuCl, CuI and their mixtures.

6. Conclusions

The structure of molten $(CuCl)_x(CuI)_{1-x}$ was investigated by using neutron diffraction. The results for CuCl show that the $g_{\alpha\beta}(r)$ functions reported by Eisenberg *et al* [28] are artificially broadened, consistent with the use by these authors of a modification function with a small k_{max} value. The RVP effective pair potentials do not reproduce the measured structure of the liquid or solid α-phase of CuI although they do give a better representation of the structure of liquid CuCl. Models for CuCl and CuI therefore need to be improved before a realistic attempt can be made to account for the structure of their mixtures. Indeed, it may well be necessary to employ *ab initio* molecular dynamics methods in order to fully understand the structure and properties of the CuCl–CuI system.

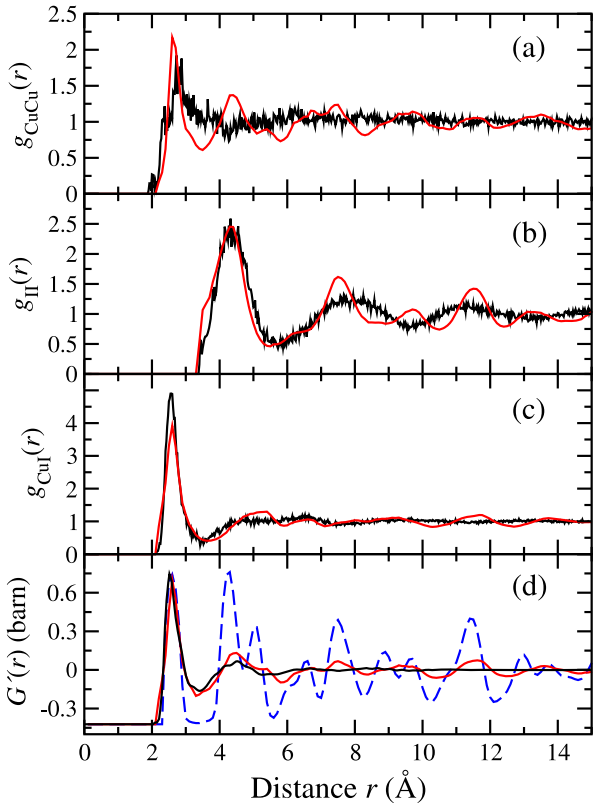

Figure 9. A comparison between the structure of the solid and liquid phases of CuI. (a)–(c) The partial pair distribution functions $g_{\alpha\beta}(r)$ for the liquid at 923 K (solid dark (black) curves), as obtained by using neutron and x-ray diffraction with RMC [50], and for the superionic α-phase at 713 K (solid light (red) curves), as obtained from an RMC analysis of neutron diffraction powder patterns [77]. (d) The neutron diffraction total pair distribution function $G'(r)$ for the liquid at 933 K (solid dark (black) curve—see figure 2), the superionic α-phase at 713 K (solid light (red) curve) as generated from the $g_{\alpha\beta}(r)$ given in (a)–(c) by using equation (3), and the zinc-blende phase at 298 K (broken (blue) curve) as generated from the $g_{\alpha\beta}(r)$ given by Chahid and McGreevy [77].

Acknowledgments

We would like to thank Daniel Bowron (ISIS) for help with the diffraction experiment, Joaquim Trullàs (UPC, Barcelona) for helpful discussions and for providing the results from his molecular dynamics simulations using the RVP potentials, Mark Wilson (Oxford) and Moises Silbert (Norwich) for helpful discussions, Robert McGreevy (ISIS), Fuyuki Shimojo (Kumamoto) and Angela Trapananti (Camerino) for providing their data sets, and the Japan Society for the Promotion of Science (JSPS) for financial support.

References

[1] Armstrong R D, Bulmer R S and Dickinson T 1973 *J. Solid State Chem.* **8** 219
[2] McGeehin P and Hooper A 1977 *J. Mater. Sci.* **12** 1
[3] Boyce J B and Huberman B A 1979 *Phys. Rep.* **51** 189
[4] Keen D A 2002 *J. Phys.: Condens. Matter* **14** R819
[5] Hull S 2004 *Rep. Prog. Phys.* **67** 1233
[6] Keen D A and Hull S 1995 *J. Phys.: Condens. Matter* **7** 5793
[7] Dejus R, Sköld K and Granéli B 1980 *Solid State Ion.* **1** 327
[8] Johansson J X M Z, Sköld K and Jørgensen J-E 1992 *Solid State Ion.* **50** 247
[9] Boyce J B, Hayes T M and Mikkelsen J C Jr 1981 *Phys. Rev.* B **23** 2876
[10] Zheng-Johansson J X M, Sköld K and Jørgensen J-E 1994 *Solid State Ion.* **70/71** 522
[11] Hull S and Keen D A 1996 *J. Phys.: Condens. Matter* **8** 6191
[12] Liu C and Angell C A 1984 *Solid State Ion.* **13** 105
[13] Bychkov E, Bolotov A, Grushko Yu, Vlasov Yu and Wortmann G 1996 *Solid State Ion.* **90** 289
[14] Bolotov A, Bychkov E, Gavrilov Yu, Grushko Yu, Pradel A, Ribes M, Tsegelnik V and Vlasov Yu 1998 *Solid State Ion.* **113–115** 697
[15] Bychkov E 2000 *Solid State Ion.* **136/137** 1111
[16] Salmon P S and Xin S 2002 *Phys. Rev.* B **65** 064202
[17] Usuki T, Nakajima K, Furukawa T, Onodera Y, Nasu T, Sakurai M and Kohara S 2006 *Solid State Ion.* **177** 2581
[18] Mönkemeyer K 1906 *Neues Jahrb. Mineral. Geol. Paläontol. Beil.* **22** 1
[19] Phillips J C 1970 *Rev. Mod. Phys.* **42** 317
[20] Madden P A and Wilson M 1996 *Chem. Soc. Rev.* **25** 339
[21] Matsunaga S 2005 *Solid State Ion.* **176** 1929
[22] Bitrián V, Trullàs J, Silbert M, Enosaki T, Kawakita Y and Takeda S 2006 *J. Chem. Phys.* **125** 184510
[23] Page D I and Mika K 1971 *J. Phys. C: Solid State Phys.* **4** 3034
[24] Powles J G 1975 *J. Phys. C: Solid State Phys.* **8** 895
[25] Gillan M J 1976 *J. Phys. C: Solid State Phys.* **9** 2261
[26] Bhatia A B and Ratti V K 1976 *J. Phys. F: Met. Phys.* **6** 927
[27] Boyce J B and Mikkelsen J C Jr 1977 *J. Phys. C: Solid State Phys.* **10** L41
[28] Eisenberg S, Jal J-F, Dupuy J, Chieux P and Knoll W 1982 *Phil. Mag.* A **46** 195
[29] Boyce J B and Mikkelsen J C Jr 1984 *Physics and Chemistry of Electrons and Ions in Condensed Matter* (*NATO-ASI Series C* vol 130) ed J V Acrivos, N F Mott and A D Yoffe (Dordrecht: Reidel) p 273
[30] Ginoza M, Nixon J H and Silbert M 1987 *J. Phys. C: Solid State Phys.* **20** 1005
[31] Takeda T, Shirakawa Y, Takesawa K, Harada S and Tamaki S 1989 *J. Phys. Soc. Japan* **58** 4007
[32] Stafford A J, Silbert M, Trullàs J and Giró A 1990 *J. Phys.: Condens. Matter* **2** 6631
[33] Trullàs J, Giró A and Silbert M 1990 *J. Phys.: Condens. Matter* **2** 6643
[34] Trullàs J, Giró A, Padró J A and Silbert M 1991 *Physica* A **171** 384
[35] Shirakawa Y, Saito M, Tamaki S, Inui M and Takeda S 1991 *J. Phys. Soc. Japan* **60** 2678
[36] Tankeshwar K and Tosi M P 1991 *J. Phys.: Condens. Matter* **3** 7511
[37] Shirakawa Y, Tamaki S, Okazaki H and Azuma M 1993 *J. Phys. Soc. Japan* **62** 544
[38] Tasseven Ç, Silbert M and Trullàs J 1995 *J. Phys.: Condens. Matter* **7** 8877
[39] Koishi T, Shirakawa Y and Tamaki S 1997 *J. Phys.: Condens. Matter* **9** 10101
[40] Howells W S 1998 *Physica* B **241–243** 329
[41] Alcaraz O and Trullàs J 2001 *J. Chem. Phys.* **115** 7071
[42] Belashchenko D K and Ostrovski O I 2002 *Calphad* **26** 523
[43] Higaki T, Tomomasa M, Hayakawa T, Chiba A and Tsuji K 2008 *J. Phys.: Condens. Matter* **20** 114106
[44] Trullàs J 2008 private communication
[45] Trullàs J, Giró A, Fontanet R and Silbert M 1994 *Phys. Rev.* B **50** 16279
[46] Waseda Y, Kang S, Sugiyama K, Kimura M and Saito M 2000 *J. Phys.: Condens. Matter* **12** A195
[47] Trapananti A, Di Cicco A and Minicucci M 2002 *Phys. Rev.* B **66** 014202

[48] Shimojo F, Aniya M and Hoshino K 2004 *J. Phys. Soc. Japan* **73** 2148
[49] Dalgic S S, Gurbuz H, Caliskan M and Ozgec O 2005 *J. Optoelectron. Adv. Mater.* **7** 2059
[50] Takeda S, Fujii H, Kawakita Y, Kato Y, Kohara S and Maruyama K 2006 *Physica* B **385/386** 249
[51] Kawakita Y, Tahara S, Fujii H, Kohara S and Takeda S 2007 *J. Phys.: Condens. Matter* **19** 335201
[52] Shimojo F, Munejiri S, Aniya M and Hoshino K 2007 *J. Non-Cryst. Solids* **353** 3505
[53] McGreevy R L and Pusztai L 1988 *Mol. Simul.* **1** 359
[54] Shirakawa Y, Tamaki S, Usuki T, Sugiyama K and Waseda Y 1994 *J. Phys. Soc. Japan* **63** 1814
[55] Inui M, Takeda S and Uechi T 1993 *J. Phys. Soc. Japan* **62** 3142
[56] Fischer H E, Barnes A C and Salmon P S 2006 *Rep. Prog. Phys.* **69** 233
[57] Lorch E 1969 *J. Phys. C: Solid State Phys.* **2** 229
[58] Salmon P S 2006 *J. Phys.: Condens. Matter* **18** 11443
[59] Salmon P S, Petri I, de Jong P H K, Verkerk P, Fischer H E and Howells W S 2004 *J. Phys.: Condens. Matter* **16** 195
[60] Soper A K 1989 *Advanced Neutron Sources* (*Inst. Phys. Conf. Ser.* vol 97) ed D K Hyer (Bristol: Institute of Physics) p 353
[61] www.isis.rl.ac.uk/disordered/Manuals/gudrun/Gudrun_manual_2006.pdf
[62] Mughabghab S F 2006 *Atlas of Neutron Resonances* 5th edn (Amsterdam: Elsevier)
[63] Salmon P S, Xin S and Fischer H E 1998 *Phys. Rev.* B **58** 6115
[64] Sears V F 1992 *Neutron News* **3** 26
[65] Inui M, Takeda S and Uechi T 1991 *J. Phys. Soc. Japan* **60** 3190
[66] Salmon P S 1994 *Proc. R. Soc.* A **445** 351
[67] McGreevy R L and Pusztai L 1990 *Proc. R. Soc.* A **430** 241
[68] Biggin S and Enderby J E 1982 *J. Phys. C: Solid State Phys.* **15** L305
[69] McGreevy R L and Howe M A 1989 *J. Phys.: Condens. Matter* **1** 9957
[70] Shannon R D 1976 *Acta Crystallogr.* A **32** 751
[71] Vashishta P and Rahman A 1978 *Phys. Rev. Lett.* **40** 1337
[72] Parrinello M, Rahman A and Vashishta P 1983 *Phys. Rev. Lett.* **50** 1073
[73] McGreevy R L and Zheng-Johansson J X M 1997 *Solid State Ion.* **95** 215
[74] Allen D A and Howe R A 1992 *J. Phys.: Condens. Matter* **4** 6029
[75] Saito M, Park C, Omote K, Sugiyama K and Waseda Y 1997 *J. Phys. Soc. Japan* **66** 633
[76] Pusztai L and McGreevy R L 1998 *J. Phys.: Condens. Matter* **10** 525
[77] Chahid A and McGreevy R L 1998 *J. Phys.: Condens. Matter* **10** 2597
[78] Barnes A C, Lague S B, Salmon P S and Fischer H E 1997 *J. Phys.: Condens. Matter* **9** 6159
[79] Barnes A C, Hamilton M A, Beck U and Fischer H E 2000 *J. Phys.: Condens. Matter* **12** 7311
[80] Vashishta P and Rahman A 1979 *Fast Ion Transport in Solids* ed P Vashishta, J N Mundy and G K Shenoy (New York: North Holland) p 527
[81] Zheng-Johansson J X M, Ebbsjö I and McGreevy R L 1995 *Solid State Ion.* **82** 115
[82] Zheng-Johansson J X M and McGreevy R L 1996 *Solid State Ion.* **83** 35
[83] McGreevy R L, Zheng-Johansson J X M and Ebbsjö I 1996 *Physica* B **226** 107
[84] Ihata K and Okazaki H 1997 *J. Phys.: Condens. Matter* **9** 1477
[85] Keen D A, Hull S, Barnes A C, Berastegui P, Crichton W A, Madden P A, Tucker M G and Wilson M 2003 *Phys. Rev.* B **68** 014117
[86] Sekkal W, Zaoui A, Laref A, Certier M and Aourag H 2000 *J. Phys.: Condens. Matter* **12** 6713
[87] Sekkal W, Aourag H and Certier M 1998 *J. Phys. Chem. Solids* **59** 1293
[88] Shimojo F and Aniya M 2003 *J. Phys. Soc. Japan* **72** 2702
[89] Bitrián V and Trullàs J 2006 *J. Phys. Chem.* B **110** 7490
[90] Bitrián V, Trullàs J and Silbert M 2007 *J. Chem. Phys.* **126** 021105
[91] Wilson M, Madden P A and Costa-Cabral B J 1996 *J. Phys. Chem.* **100** 1227